CrystEngComm

PAPER

View Article Online
View Journal

Check for updates

Cite this: DOI: 10.1039/d5ce00956a

Hydrogen-bonded salt cocrystals of xenon difluoride and protonated perfluoroamides†

Erik Uran [a,b] and Matic Lozinšek *[a,b]

Received 3rd October 2025,
Accepted 31st October 2025

DOI: 10.1039/d5ce00956a

rsc.li/crystengcomm

The hydrogen-bonding ability of XeF_2 is an important factor influencing its chemical properties and reactivity, yet structurally characterised examples of hydrogen-bonded xenon fluorides remain rare. In this work, three salt cocrystals containing hydrogen-bonded xenon difluoride and hexafluoridoarsenate salts of protonated perfluoroamides—$CF_3C(OH)NH_2[AsF_6]{\cdot}XeF_2$, $C_2F_5C(OH)NH_2[AsF_6]{\cdot}XeF_2$, and $C_3F_7C(OH)NH_2[AsF_6]{\cdot}XeF_2$—were synthesised and structurally characterised. Diverse hydrogen-bonding motifs were observed, and the first crystallographically characterised examples of N–H⋯FXeF hydrogen bonds are presented. In total, eleven new crystal structures are reported, including two perfluoroamides, three protonated and two hemiprotonated perfluoroamides, and one salt cocrystal containing an oxonium ion. The XeF_2-containing cocrystals demonstrate that XeF_2 reliably functions as a hydrogen-bond acceptor and readily forms hydrogen-bonded cocrystals. These findings broaden the scope of noble-gas chemistry and highlight the potential of noble-gas fluorides for cocrystal formation.

Introduction

Xenon difluoride (XeF_2) is the most common and extensively studied binary noble-gas fluoride and serves as a precursor to a wide range of xenon compounds.[1,2] It is a nonpolar molecular compound with linear geometry. XeF_2 is a good fluoride-ion donor[3] and thus forms a variety of Lewis acid–base adducts[4] and a plethora of coordination compounds with metal cations.[1,2,5]

The ability of XeF_2 to act as a hydrogen-bond acceptor strongly influences its physical and chemical properties. As a nonpolar molecule, it is highly soluble in the polar protic solvent anhydrous HF (aHF) (167 g/100 g at 30 °C).[6] This unusually high solubility arises from the formation of FXe–F⋯HF hydrogen bonds.[7–9] Furthermore, XeF_2 dissolved in aHF is a considerably more potent oxidiser than pure XeF_2, and even trace amounts of HF can catalyse its reactions with organic substrates through the hydrogen-bonding induced polarisation $[FXe^{\delta+}–F^{\delta-}{\cdots}HF]$.[10] HF also facilitates fluorine exchange in XeF_2, enabling the synthesis of ^{18}F-radiolabelled XeF_2.[11,12] In certain cases, the influence of HF is so pronounced that it can unexpectedly alter reaction outcomes, even when inadvertently generated by reaction with the vessel material.[13]

Despite the ability of XeF_2 to act as a hydrogen-bond acceptor, systematic crystallographic investigations are absent, and reported solid-state examples remain scarce. To date, only a handful of crystallographically characterised examples of hydrogen-bonded XeF_2 have been described. These include O–H⋯FXeF hydrogen bonds observed in $H_3O[AsF_6]{\cdot}2XeF_2$ and in $HNO_3{\cdot}XeF_2$ cocrystals,[14,15] as well as an F–H⋯FXeF interaction observed in the coordination complex $[Cd(HF)_2(XeF_2)(MF_6)_2]$ (M = Ta, Nb).[5,16]

It has also been shown spectroscopically that protonated trifluoroacetamide (CF_3CONH_2) forms a hydrogen-bonded salt cocrystal[17] with XeF_2, $CF_3C(OH)NH_2[AsF_6]{\cdot}XeF_2{\cdot}x$HF.[18] This cocrystal is particularly noteworthy, as it may feature both $=OH^+$ and $–NH_2$ groups as hydrogen-bond donors,[18] potentially offering insight into the hydrogen-bonding preferences of XeF_2.

To investigate the hydrogen-bonding propensity of XeF_2 in the solid state and its tendency to form cocrystals with NH and OH hydrogen-bond donors, the crystal structures of XeF_2 salt cocrystals with protonated CF_3CONH_2, $C_2F_5CONH_2$, and $C_3F_7CONH_2$ were studied in this work. The perfluoroamides were selected because of their anticipated resistance to oxidative-fluorination by XeF_2.

Results and discussion

Crystal structures of $CF_3CF_2CONH_2$ and $CF_3CF_2CF_2CONH_2$

The crystal structures of pentafluoropropionamide ($C_2F_5CONH_2$) and heptafluorobutyramide ($C_3F_7CONH_2$) were elucidated by low-temperature single-crystal X-ray diffraction (LT SCXRD)

[a] Extreme Condition Chemistry Laboratory (ECCL K2), Jožef Stefan Institute, Jamova cesta 39, 1000 Ljubljana, Slovenia. E-mail: matic.lozinsek@ijs.si
[b] Jožef Stefan International Postgraduate School, Jamova cesta 39, 1000 Ljubljana, Slovenia

† Dedicated to Professor Resnati, celebrating a career in fluorine and noncovalent chemistry on the occasion of his 70th birthday.

Table 1 Summary of crystal data and refinement results for crystal structures of amides and protonated amides

Compound	$C_2F_5CONH_2$	$C_3F_7CONH_2$	$CF_3C(OH)NH_2[AsF_6]$	$C_2F_5C(OH)NH_2[AsF_6]$	$C_3F_7C(OH)NH_2[AsF_6]$
Space group	$C2/c$	$P\bar{1}$	$P2_1/c$	$Pccn$	$P2_1/c$
a (Å)	21.7871(5)	5.11713(18)	9.81910(18)	8.12957(13)	6.17592(15)
b (Å)	5.11704(12)	5.27137(14)	7.90095(13)	25.2768(4)	7.94187(19)
c (Å)	10.0754(3)	12.7768(3)	20.5015(4)	9.34322(16)	21.7914(5)
α (°)	90	95.467(2)	90	90	90
β (°)	98.140(2)	91.890(3)	98.6498(18)	90	96.014(2)
γ (°)	90	105.584(3)	90	90	90
V (Å^3)	1111.94(5)	329.847(18)	1572.42(5)	1919.93(5)	1062.95(4)
M	163.06	213.07	302.97	352.98	402.99
Z	8	2	8	8	4
T (K)	100	100	100	100	100
$R[F^2 > 2\sigma(F^2)]$	0.048	0.028	0.033	0.027	0.027
w$R(F^2)$	0.138	0.076	0.087	0.058	0.068

(Tables 1 and S1), whereas the crystal structure of CF_3CONH_2 has been previously reported at 295 K and 110 K.[19,20] For comparison of bond lengths (Table S2), only the structure obtained at 110 K was considered.[20]

$C_2F_5CONH_2$ (Fig. 1a and S1) crystallizes in the monoclinic space group $C2/c$ with Z = 8. The C=O bond length (1.2323(19) Å) is comparable to the distances observed in the crystal structures of other primary amides, and the same applies to the C–N bond (1.317(2) Å).[21] Two N–H⋯O hydrogen bonds (2.912(2) Å, 171(2)°; 2.8396(17) Å, 149(2)°; Table S3) in the crystal structure form $R_2^2(8)$ and $R_6^4(16)$ hydrogen-bonding motifs,[22] which assemble into a corrugated layer parallel to the bc plane (Fig. S2 and S3).

$C_3F_7CONH_2$ (Fig. 1b and S4) crystallizes in the triclinic space group $P\bar{1}$ with Z = 2. The C=O bond distance (1.2293(15) Å) is essentially identical to that in $C_2F_5CONH_2$, as is the C–N bond (1.3162(16) Å). These bond distances are shorter than the corresponding ones observed in non-fluorinated secondary amides, such as capsaicin.[23] Two N–H⋯O hydrogen bonds (Table S4) are present in the crystal structure (2.9313(14) Å, 174.3(16)°; 2.8495(14) Å, 140.4(15)°), which fall within the typical range for amide molecules.[21] The $R_2^2(8)$ and $R_4^2(8)$ hydrogen-bond motifs link the molecules into a ladder along the a-crystallographic axis (Fig. S5).

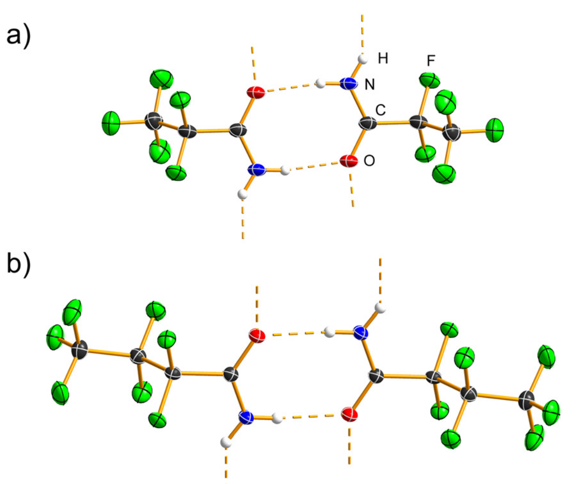

Fig. 1 $R_2^2(8)$ hydrogen-bonding motifs in the crystal structures of (a) $C_2F_5CONH_2$ and (b) $C_3F_7CONH_2$. Hydrogen bonds are shown as dashed orange lines. Displacement ellipsoids are drawn at the 50% probability level, and hydrogen atoms are represented as spheres of arbitrary radius.

Protonation of amides in superacidic media HF–AsF_5

All amides are soluble in aHF and readily undergo protonation upon addition of AsF_5. In all cases, protonation occurs at the oxygen atom, consistent with previous observations.[18,24–26] Low-temperature crystallisation from aHF afforded crystals of suitable quality for SCXRD.

$CF_3C(OH)NH_2[AsF_6]$ (Tables 1, S1 and S2; Fig. S6) crystallises in the monoclinic space group $P2_1/c$ with Z = 8 and Z' = 2. Upon protonation, the C=O bonds (1.2795(19), 1.282(2) Å) lengthen and the C–N bonds (1.279(2), 1.281(2) Å) shorten relative to those in CF_3CONH_2 (1.2304(12) and 1.3164(13) Å, respectively).[20] These changes in the C=O and C–N bond lengths are consistent with previous crystallographic studies of protonated amides.[25–27] The O–H⋯F hydrogen bonds (2.5860(16) Å, 2.6530(18) Å; Table S5) bracket the value observed in $CF_3C(OH)NH_2[SbF_6]$ (2.600(1) Å), whereas the N–H⋯F hydrogen bonds (2.8236(18)–3.0797(18) Å) are comparable to those in $CF_3C(OH)NH_2[SbF_6]$ (2.884(2), 2.933(2) Å).[26] All hydrogen-bond angles (121(2)–179(3)°) fall within the typical range. The $[AsF_6]^-$ anions deviate from ideal octahedral geometry, with the longest As–F bonds (1.7524(10), 1.7557(10) Å) participating in hydrogen bonding with $=OH^+$ group. In the crystal structure, cations and anions are linked through O–H⋯F and N–H⋯F hydrogen-bonded chains (Fig. 2a and S7).

$C_2F_5C(OH)NH_2[AsF_6]$ (Tables 1, S1 and S2) crystallises in the orthorhombic space group $Pccn$ with Z = 8 and features a disordered $-C_2F_5$ moiety (Fig. S8). Perfluorinated alkyl chains frequently exhibit disorder in the crystalline state,[28] as F⋯F interactions are relatively weak,[29] and can therefore adopt various conformations. The C=O (1.2821(15) Å) and C–N (1.2772(16) Å) bonds are longer and shorter, respectively, than those in $C_2F_5CONH_2$. The $[AsF_6]^-$ anion deviates from ideal octahedral geometry, with the mer-As–F bonds involved

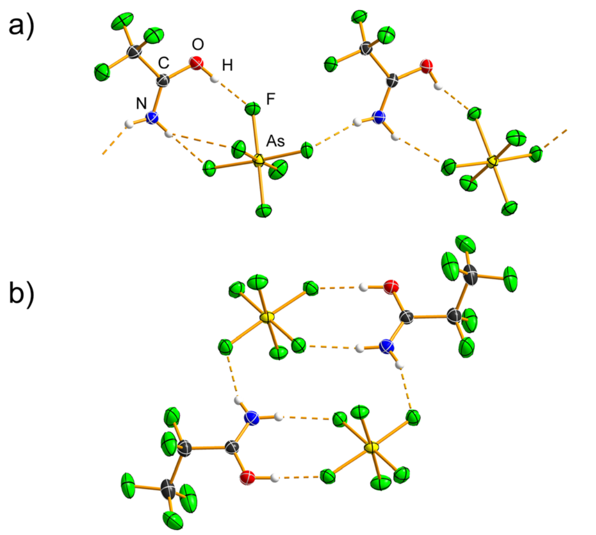

Fig. 2 Crystal structure of (a) the hydrogen-bonded chain in $CF_3C(OH)NH_2[AsF_6]$ and (b) the discrete hydrogen-bonded cluster in $C_2F_5C(OH)NH_2[AsF_6]$ (only one orientation of the disordered $-C_2F_5$ unit is shown). Hydrogen bonds are shown as dashed orange lines. Displacement ellipsoids are drawn at the 50% probability level, and hydrogen atoms are represented as spheres of arbitrary radius.

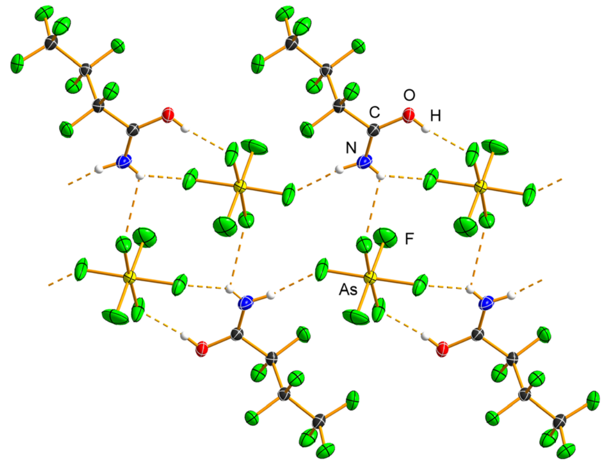

Fig. 3 Hydrogen-bonded ribbon in $C_3F_7C(OH)NH_2[AsF_6]$ (only one orientation of the disordered $[AsF_6]^-$ anion is shown). Hydrogen bonds are shown as dashed orange lines. Displacement ellipsoids are drawn at the 50% probability level, and hydrogen atoms are represented as spheres of arbitrary radius.

in hydrogen bonding being longer (1.7253(8)–1.7453(8) Å) than the remaining As–F bonds (1.6976(8)–1.7111(8) Å). The hydrogen bonds (Table S6) between the $=OH^+$ and $-NH_2$ groups and the $[AsF_6]^-$ anions (O(H)···F, 2.6006(12) Å, 172(2)°; N(H)···F, 2.8309(13) Å, 174(2)° and 2.8316(14) Å, 161.3(19)°) lead to the formation of discrete units (Fig. 2b, S8 and S9), exhibiting $R_2^2(8)$ and $R_4^4(12)$ hydrogen-bonding motifs.

$C_3F_7C(OH)NH_2[AsF_6]$ (Tables 1, S1 and S2) crystallises in the monoclinic space group $P2_1/c$ with Z = 4, with the $[AsF_6]^-$ anion disordered over two positions (Fig. S10). The C=O bond (1.2797(14) Å) is elongated, and the C–N bond (1.2841(16) Å) is shortened compared to those in $C_3F_7CONH_2$. A similar C=O(H) bond distance (1.274(2) Å) was observed in the crystal structure of $(C_6F_5)_2COH[AsF_6]$.[30] Hydrogen bonds (Table S7) are formed between the $=OH^+$ group (2.541(3), 2.557(3) Å; 157(3), 165(3)°) or the $-NH_2$ group (2.737(4)–3.179(5) Å, 118.0(19)–168.1(19)°) and the $[AsF_6]^-$ anions. The O···F hydrogen bond is the shortest among the protonated amides in this study, and also shorter than those in $CH_3C(OH)NH_2[AsF_6]$[25] and $CF_3C(OH)NH_2[SbF_6]$.[26] The $[AsF_6]^-$ anion deviates from ideal octahedral geometry (1.642(3)–1.795(2) Å). The $C_3F_7C(OH)NH_2^+$ cations and $[AsF_6]^-$ anions are linked into a hydrogen-bonded ribbon (Fig. 3 and S11), exhibiting conjoined $R_4^4(12)$, $R_2^4(8)$ and $R_2^2(8)$ motifs.

Two hemiprotonated salts, $(CF_3CONH_2)_2H[AsF_6]$ and $(C_3F_7CONH_2)_2H[AsF_6]$ (Fig. 4 and S12–S17; Tables 2, S1 and S2), were also crystallographically characterised. The former was inadvertently found during the low-temperature crystal selection and mounting of the $CF_3C(OH)NH_2[AsF_6]\cdot XeF_2$ sample, whereas the latter was identified as an impurity in the sample of $C_3F_7C(OH)NH_2[AsF_6]\cdot XeF_2$ salt cocrystals. Both compounds crystallise in the triclinic space group $P\bar{1}$ with Z = 2. In both structures, the C=O bonds are elongated (1.283(6) Å in $(CF_3CONH_2)_2H[AsF_6]$; 1.2652(9), 1.2459(9) Å in $(C_3F_7CONH_2)_2H[AsF_6]$), whereas the C–N bonds are shortened (1.274(7) Å in $(CF_3CONH_2)_2H[AsF_6]$; 1.2942(10), 1.3027(10) Å in $(C_3F_7CONH_2)_2H[AsF_6]$) compared to the non-protonated amides.[20] The values for one of the amide molecules in $(CF_3CONH_2)_2H[AsF_6]$ fall within the

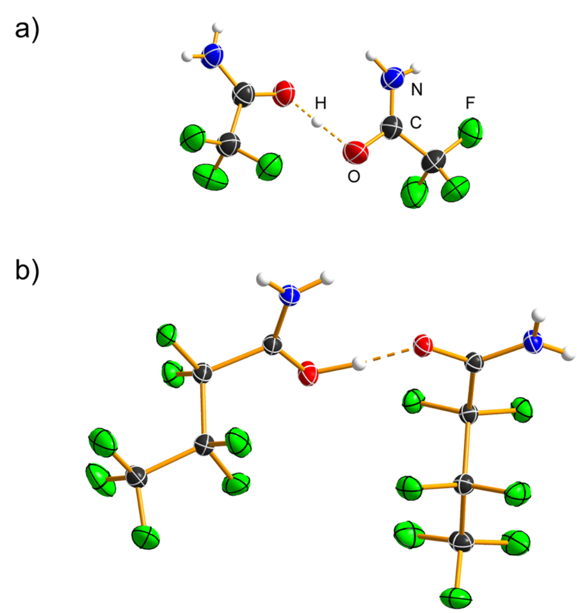

Fig. 4 Hydrogen-bonded dimers in the crystal structure of (a) $(CF_3CONH_2)_2H[AsF_6]$ and (b) $(C_3F_7CONH_2)_2H[AsF_6]$. The short O–H···O=C hydrogen bonds are shown as dashed orange lines. Displacement ellipsoids are drawn at the 50% probability level, and hydrogen atoms are represented as spheres of arbitrary radius.

Table 2 Summary of crystal data and refinement results for hemiprotonated amides and $H_3O[AsF_6]\cdot 2CF_3CONH_2$ salt cocrystal

Compound	$(CF_3CONH_2)_2H[AsF_6]$	$(C_3F_7CONH_2)_2H[AsF_6]$	$H_3O[AsF_6]\cdot 2CF_3CONH_2$
Space group	$P\bar{1}$	$P\bar{1}$	*Pnma*
a (Å)	5.2815(3)	5.32051(4)	11.5349(2)
b (Å)	10.1517(6)	10.45222(9)	14.0649(3)
c (Å)	12.4911(6)	16.10170(12)	7.78994(14)
α (°)	108.936(5)	90.5740(6)	90
β (°)	93.107(5)	90.8760(6)	90
γ (°)	102.904(5)	103.0402(7)	90
V (Å^3)	611.63(6)	872.156(12)	1263.82(4)
M	416.02	616.06	434.04
Z	2	2	4
T (K)	100	100	100
$R[F^2 > 2\sigma(F^2)]$	0.047	0.022	0.037
w$R(F^2)$	0.125	0.055	0.085

range for neutral amide,[20] owing to the relatively high standard uncertainties of the bond lengths. The O(H)⋯O hydrogen bond length in $(CF_3CONH_2)_2H[AsF_6]$ (2.426(5) Å, 170(8)°) is essentially identical to that in $(C_3F_7CONH_2)_2H[AsF_6]$ (2.4174(9) Å, 172(2)°) (Tables S8 and S9), and comparable to literature values for such hydrogen-bonded systems.[21] The nearly equidistant position of the hydrogen atom (O–H, H⋯O: 1.13(9), 1.31(9) Å in $(CF_3CONH_2)_2H[AsF_6]$; 1.06(2), 1.36(2) Å in $(C_3F_7CONH_2)_2H[AsF_6]$), together with the relatively short O⋯O distances, indicates strong, positive charge-assisted hydrogen bonding, (+) CAHB.[31] These structures represent rare examples of proton sharing between two primary amide molecules,[21,32] a motif more commonly observed in secondary and tertiary amides.[21] The $-NH_2$ groups are hydrogen-bonded to $[AsF_6]^-$ anions (N⋯F, 2.644(5)–3.005(5) Å in $(CF_3CONH_2)_2H[AsF_6]$; 2.8168(9)–3.1046(9) Å in $(C_3F_7CONH_2)_2H[AsF_6]$) (Fig. S13–S17), resulting in the formation of ribbons that are further interconnected by the anions into layers parallel to the *ab* plane.

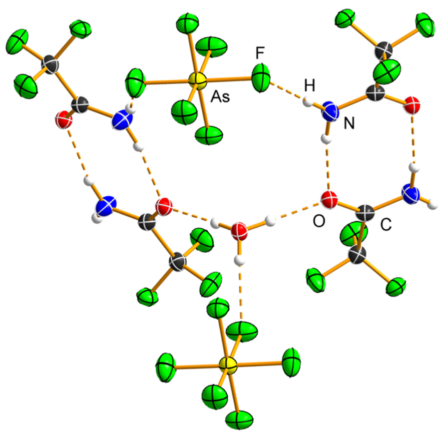

Fig. 5 $R_6^4(14)$ hydrogen-bonded cluster in the crystal structure of the $H_3O[AsF_6]\cdot 2CF_3CONH_2$ salt cocrystal. Hydrogen bonds are shown by dashed orange lines. Displacement ellipsoids are drawn at the 50% probability level, and hydrogen atoms are represented as spheres of arbitrary radius.

A crystal of $H_3O[AsF_6]\cdot 2CF_3CONH_2$ (Tables 2, S1 and S2; Fig. 5 and S18–S20) was fortuitously found during the low-temperature crystal selection and mounting of the $CF_3C(OH)NH_2[AsF_6]\cdot XeF_2$ sample. It crystallises in the orthorhombic space group *Pnma* with $Z = 4$. The amide molecule is not protonated, resulting in C=O (1.236(4) Å) and C–N (1.304(4) Å) bond lengths that are close to those in CF_3CONH_2.[20] The amide molecule acts as both a hydrogen-bond donor and acceptor (Table S10, Fig. S19), forming N–H⋯F(As) and N–H⋯O(C) hydrogen bonds. An $R_2^2(8)$ motif is observed between two amide molecules, with the N⋯O hydrogen bond (2.959(4) Å, 171(4)°) comparable to that found in CF_3CONH_2.[20] The H_3O^+ cation forms three hydrogen bonds: two symmetrically equivalent O–H⋯O(C) (2.525(3) Å, 167(4)°) and one O–H⋯F hydrogen bond (2.657(5) Å, 173(7)°) with the $[AsF_6]^-$ anion. Together, these hydrogen bonds form a hydrogen-bonded cluster represented by $R_6^6(20)$, $R_6^4(14)$ and $R_2^2(8)$ graph-set motifs[22] (Fig. 5), which further extend into a layer parallel to the *bc* plane (Fig. S20).

Hydrogen-bonded salt cocrystals of XeF_2

The reaction of amides with equimolar amounts of $[XeF][AsF_6]$ at temperatures down to −30 °C leads to the formation of $RC(OH)NH_2[AsF_6]\cdot XeF_2$ salt cocrystals. This indicates that a proton from HF is transferred to the amide, generating a protonated amide, while the resulting fluoride anion reacts with $[XeF]^+$ to form XeF_2. This behaviour was also reported in a previous study of the CF_3CONH_2–$[XeF][AsF_6]$ system.[18]

The salt cocrystals (Tables 3, S1 and S2) thus feature protonated amides cocrystallised with XeF_2 and exhibit a rare O–H⋯FXeF hydrogen bond, as well as the first crystallographically characterised examples of N–H⋯FXeF hydrogen bonds.

$CF_3C(OH)NH_2[AsF_6]\cdot XeF_2$ (Fig. 6 and S21) crystallises in the monoclinic space group $P2_1/n$ with $Z = 4$. The XeF_2 molecule exhibits slight asymmetry in Xe–F bond distances (1.9669(10), 2.0237(9) Å) compared to pure XeF_2 (1.999(4) Å),[33] and it remains linear (178.10(5) Å). The asymmetry of XeF_2 is slightly smaller than that observed in $XeF_2\cdot HNO_3$ (1.9737(8), 2.0506(8) Å).[15]

Table 3 Summary of crystal data and refinement results for salt cocrystals of protonated amides with XeF_2

Compound	$CF_3C(OH)NH_2[AsF_6]\cdot XeF_2$	$C_2F_5C(OH)NH_2[AsF_6]\cdot XeF_2$	$C_3F_7C(OH)NH_2[AsF_6]\cdot XeF_2$
Space group	$P2_1/n$	$Aea2$	$Pnna$
a (Å)	7.41785(9)	8.67561(10)	8.62011(14)
b (Å)	9.84875(11)	31.0125(4)	35.5418(5)
c (Å)	14.90113(17)	8.65174(9)	8.71910(12)
α (°)	90	90	90
β (°)	99.4517(11)	90	90
γ (°)	90	90	90
V (Å^3)	1073.85(2)	2327.77(4)	2671.31(7)
M	472.27	522.28	572.29
Z	4	8	8
T (K)	100	100	100
$R[F^2 > 2\sigma(F^2)]$	0.025	0.018	0.026
w$R(F^2)$	0.067	0.038	0.066

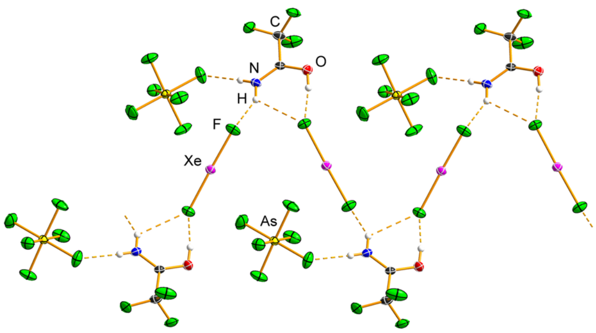

Fig. 6 Hydrogen-bonded ribbon in the crystal structure of the salt cocrystal $CF_3C(OH)NH_2[AsF_6]\cdot XeF_2$. Only one orientation of the disordered $-CF_3$ moiety is shown. Hydrogen bonds are shown as dashed orange lines. Displacement ellipsoids are drawn at the 50% probability level, and hydrogen atoms are represented as spheres of arbitrary radius.

$CF_3C(OH)NH_2[AsF_6]\cdot XeF_2$ is the only salt cocrystal in this series that exhibits both O–H⋯F(Xe) and N–H⋯F(Xe) hydrogen bonds. One fluorine atom of XeF_2 is acting as a bifurcated acceptor (Fig. 6 and S21; Table S11). The O–H⋯F(Xe) hydrogen bond (2.5467(14) Å, 171(3)°) is shorter than that in $H_3O[AsF_6]\cdot 2XeF_2$ (2.571(3) Å)[14] and $HNO_3\cdot XeF_2$ (2.690(1) Å).[15] It is also significantly shorter than the O–H⋯F(As) hydrogen bonds in $CF_3C(OH)NH_2[AsF_6]$ and $C_2F_5C(OH)NH_2[AsF_6]$, but comparable to that in $C_3F_7C(OH)NH_2[AsF_6]$. The N–H⋯F(Xe) hydrogen bonds (2.7865(15) Å, 151(3)°; 3.0894(16), 124(2)°), which involve a single bifurcated donor, are longer than those observed in the other two salt cocrystals described in this study. The C=O (1.2773(15) Å) and C–N (1.2772(16) Å) bond lengths are essentially identical to those in the protonated salts,[26] indicating a negligible influence of hydrogen bonding on the overall geometry of the $CF_3C(OH)NH_2^+$ cation. The $-CF_3$ moiety is disordered, as also observed in the crystal structure of CF_3CONH_2.[20] The $[AsF_6]^-$ anion participates in hydrogen bonding with the $-NH_2$ group (2.8270(18) Å, 176(3)°; 3.0594(15) Å, 111(2)°), resulting in a slight deviation from ideal octahedral geometry (As–F, 1.7006(12)–1.7417(11) Å).

Hydrogen bonds between $CF_3C(OH)NH_2^+$ and XeF_2 form a zigzag chain parallel to the b-crystallographic axis, with pendant $[AsF_6]^-$ anions connected to the chain *via* N–H⋯F(As) hydrogen bonds, giving rise to a ribbon-like structure (Fig. 6 and S22).

Both $C_2F_5C(OH)NH_2[AsF_6]\cdot XeF_2$ and $C_3F_7C(OH)NH_2[AsF_6]\cdot XeF_2$ (Tables 3, S1 and S2; Fig. S23–S26) crystallise in orthorhombic space groups, $Aea2$ and $Pnna$, respectively, with Z = 8. The asymmetry of the Xe–F bond lengths in $C_2F_5C(OH)NH_2[AsF_6]\cdot XeF_2$ (1.9734(14), 2.0061(15) Å) and in $C_3F_7C(OH)NH_2[AsF_6]\cdot XeF_2$ (1.9674(15), 2.0135(16) Å) is comparable. The shorter Xe–F bonds are similar to that observed in the trifluoroacetamide analogue, whereas the longer Xe–F bonds are significantly shorter. In both cocrystals, the F–Xe–F angle is essentially linear (179.88(9)°; 179.57(7)°).

The N–H⋯F(Xe) hydrogen bonds (Tables S12 and S13) in $C_2F_5C(OH)NH_2[AsF_6]\cdot XeF_2$ (2.688(3), 2.729(3) Å) and $C_3F_7C(OH)NH_2[AsF_6]\cdot XeF_2$ (2.692(3), 2.737(3) Å) are comparable and are significantly shorter than the corresponding hydrogen bonds in $CF_3C(OH)NH_2[AsF_6]\cdot XeF_2$. The C=O (1.289(2), 1.285(3) Å) and C–N (1.279(3), 1.280(3) Å) bond lengths in $C_2F_5C(OH)NH_2[AsF_6]\cdot XeF_2$ and $C_3F_7C(OH)NH_2[AsF_6]\cdot XeF_2$ are almost identical to those observed in the corresponding protonated salts.

The protonated oxygen atom acts as a hydrogen-bond donor towards the $[AsF_6]^-$ anions, forming bifurcated hydrogen bonds (Fig. 7, S23 and S25), which are longer than the O–H⋯F(As) hydrogen bonds observed in the parent protonated salts.

The packing in both $C_2F_5C(OH)NH_2[AsF_6]\cdot XeF_2$ and $C_3F_7C(OH)NH_2[AsF_6]\cdot XeF_2$ consists of hydrogen-bonded ribbons composed of alternating protonated amide and XeF_2 molecules, similar to those observed in $CF_3C(OH)NH_2[AsF_6]\cdot XeF_2$. These ribbons are further connected by O–H⋯F(As) hydrogen bonds, and in the case of $C_3F_7C(OH)NH_2[AsF_6]\cdot XeF_2$, also by N–H⋯F(As) hydrogen bonds (Fig. S24 and S26).

The relatively small difference in Xe–F bond lengths in the present XeF_2 cocrystals suggests that hydrogen bonding has only a minor influence on XeF_2 ionisation ($XeF_2 \rightarrow XeF^+ +$

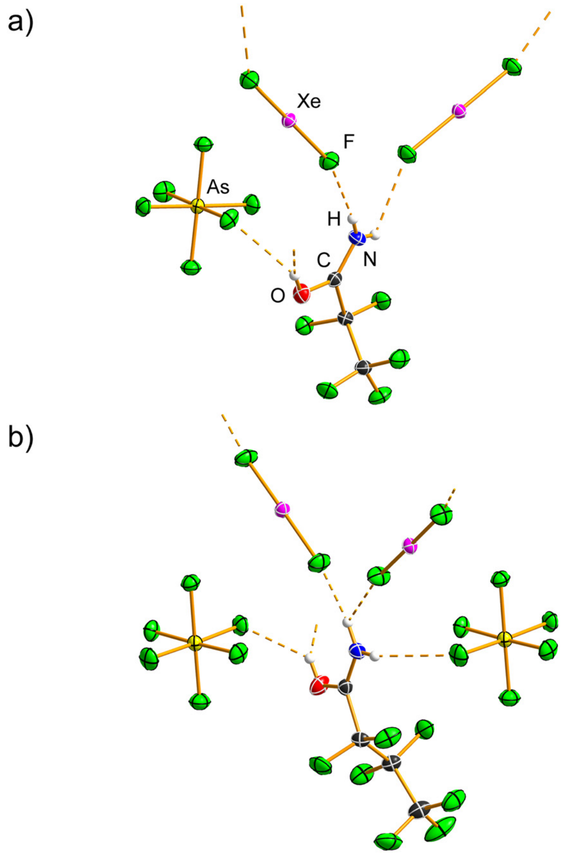

Fig. 7 Hydrogen bonds (dashed orange lines) in the crystal structures of the salt cocrystals (a) $C_2F_5C(OH)NH_2[AsF_6]·XeF_2$ and (b) $C_3F_7C(OH)NH_2[AsF_6]·XeF_2$. The OH groups are bifurcated hydrogen-bond donors; however, two $[AsF_6]^-$ anions have been omitted for clarity. Displacement ellipsoids are drawn at the 50% probability level, and hydrogen atoms are represented as spheres of arbitrary radius.

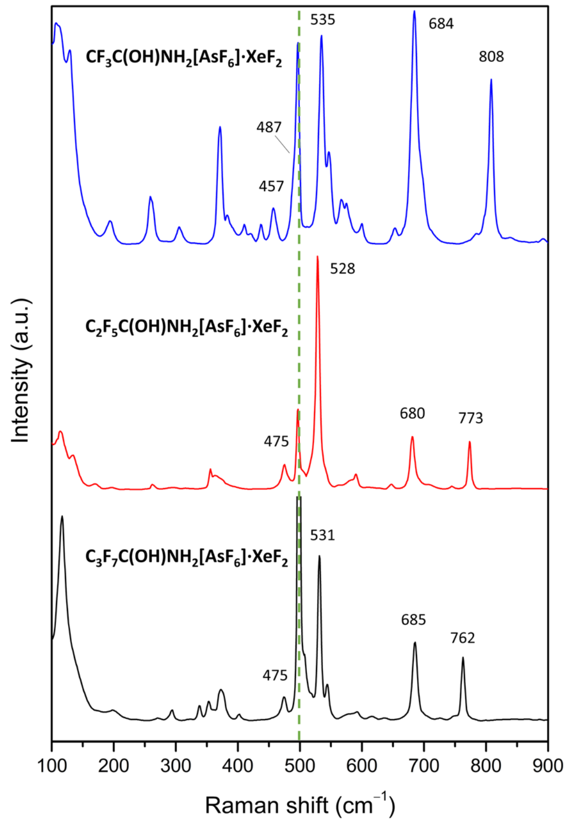

Fig. 8 Raman spectra of XeF_2 salt cocrystals with protonated amides recorded at low temperatures (−90 °C). The green dashed line is placed at the position of free XeF_2 (497 cm^{-1})[41] which was observed as an impurity in the reactions.

F^-).[34] In particular, the shorter Xe–F bonds (1.9669(10)–1.9734(14) Å) are considerably longer than those found in $[XeF]^+$ tight ion pairs[33,35,36] and in $[Xe_2F_3]^+$ salts.[35,37] They are comparable to the shortest Xe–F bond lengths in XeF_2 adduct-salts with $[BrOF_2]^+$ (1.956(5), 1.960(4) Å)[38] and $[BrO_2]^+$ cations (1.970(4)–1.978(3) Å).[39] Nevertheless, the distortion of hydrogen-bonded XeF_2 observed in the present salt cocrystals is significant when compared with Xe–F bond distances observed in the crystal structures containing cocrystallised XeF_2, *e.g.*, $3XeF_2·2MnF_4$ (1.9933(7) Å),[36] and in the molecular cocrystals $XeF_2·XeF_4$ (1.9940(9) Å)[37] and $XeF_2·XeOF_4$ (2.014(5) Å),[40] in which XeF_2 is centrosymmetric.

Vibrational spectroscopy

To corroborate the findings from LT SCXRD and to gain further insight into the ionisation of XeF_2, low-temperature Raman spectra were measured (Fig. 8 and S27–S40). Two bands at 457–475 and 528–535 cm^{-1} are observed in all XeF_2 salt cocrystals in this study, corresponding to the elongated and shortened Xe–F bond, respectively. These bands are significantly shifted from that of pure XeF_2 (497 cm^{-1})[41] and from values observed when cocrystallised XeF_2 does not participate in significant intermolecular interactions, such as in $XeF_2·XeOF_4$ (494, 503 cm^{-1}),[40] $XeF_2·XeF_4$ (505 cm^{-1}),[42] $3XeF_2·2MnF_4$ (508 cm^{-1}),[36] and $XeF_2·N_2O_4$ (509 cm^{-1}).[15] The value of the higher-frequency band is comparable to the Raman shifts reported for the adduct salts $[BrOF_2][AsF_6]·XeF_2$ (531, 543, 559 cm^{-1}),[38] $[BrO_2][AsF_6]·nXeF_2$ (n = 1, 2; 516–546 cm^{-1}),[39] and for the hydrogen-bonded cocrystals $H_3O[AsF_6]·2XeF_2$ (552 cm^{-1})[14] and $HNO_3·XeF_2$ (529 cm^{-1}).[15] However, these shifts are significantly smaller than those observed in $[XeF]^+$ tight-ion pair salts (>600 cm^{-1}) and $[Xe_2F_3]^+$ cations (580–600 cm^{-1}).[1,33,35,36,43,44] The band around 535 cm^{-1} is particularly noteworthy, as this value coincides with that observed for XeF_2 dissolved in aHF, which has been attributed to the FXe–F···HF hydrogen bonds.[7–9]

In addition to the bands attributed to XeF_2, those arising from $[AsF_6]^-$ anions are observed around 375 and 680 cm^{-1}.[18,25,26,45] Vibrations from the protonated amide molecules are also present, including an intense band around 800 cm^{-1} corresponding to ν(C–C),[25,26] and peaks near 1100 cm^{-1} attributed to C–F vibrations.[18,26,46] In all protonated amides, the N–H stretching vibrations were observed in 3150–3400 cm^{-1} range.[18,26,46]

Experimental

Caution! Anhydrous HF, AsF_5, XeF_2, $[XeF][AsF_6]$ and the compounds prepared in this study are highly reactive and hazardous. The amides used may cause skin, eye, and respiratory irritation. Contact with the skin must be avoided, and all compounds should be handled exclusively in a well-ventilated fume hood.

Appropriate safety precautions must be observed at all times, and working with minimal quantities is strongly recommended.

Materials and methods

Reactions were carried out in fluorinated ethylene propylene (FEP) vessels equipped with Kel-F or PTFE valves. All vessels were passivated with fluorine prior to use. Volatile substances were handled using a fluorine-resistant metal vacuum line, whereas solids were manipulated inside an N_2-filled glovebox. Detailed synthetic procedures are provided in the SI. Characterisation was performed by low-temperature single-crystal X-ray diffraction and low-temperature Raman spectroscopy. Single-crystal selection and mounting were carried out using a low-temperature crystal-mounting apparatus, as described previously (SI).[30,36,47] Low-temperature Raman spectra were recorded directly on the aluminium trough used for mounting single crystals for X-ray diffraction measurements.

Conclusions

In this work, the perfluoroamides trifluoroacetamide (CF_3CONH_2), pentafluoropropionamide ($C_2F_5CONH_2$), and heptafluorobutyramide ($C_3F_7CONH_2$), were protonated in superacidic medium HF–AsF_5, and the crystal structures of the resulting salts, $CF_3C(OH)NH_2[AsF_6]$, $C_2F_5C(OH)NH_2[AsF_6]$, and $C_3F_7C(OH)NH_2[AsF_6]$ were elucidated. Protonation at the carbonyl oxygen atom is consistently observed. In addition, the crystal structures of the amides $C_2F_5CONH_2$ and $C_3F_7CONH_2$, the hemiprotonated salts $(CF_3CONH_2)_2H[AsF_6]$ and $(C_3F_7CONH_2)_2H[AsF_6]$, and the oxonium salt cocrystal $H_3O[AsF_6]\cdot 2CF_3CONH_2$ were determined. Low-temperature reactions of the perfluoroamides with $[XeF][AsF_6]$ in aHF yielded rare XeF_2-containing salt cocrystals: $CF_3C(OH)NH_2[AsF_6]\cdot XeF_2$, $C_2F_5C(OH)NH_2[AsF_6]\cdot XeF_2$ and $C_3F_7C(OH)NH_2[AsF_6]\cdot XeF_2$. Their crystal structures reveal a rare example of O–H⋯FXeF and the first crystallographically characterised cases of N–H⋯FXeF hydrogen bonding. The XeF_2 molecule is slightly polarised, as indicated by the differences observed in Xe–F bond lengths compared with those in free XeF_2; this finding is corroborated by low-temperature Raman spectroscopy. The reported crystal structures display diverse hydrogen-bonding motifs involving O–H⋯F(Xe), N–H⋯F(Xe), O–H⋯F(As) and N–H⋯F(As) interactions. The salt cocrystals prepared and structurally characterised in this study demonstrate that XeF_2 readily forms hydrogen-bonded cocrystals and serves as a reliable hydrogen-bond acceptor. These results open new possibilities for the exploration of cocrystal formation with noble-gas fluorides and the expansion of noble-gas chemistry.

Author contributions

Conceptualization, data curation, formal analysis, investigation, visualization, writing – original draft: EU; funding acquisition, methodology, project administration, resources, supervision: ML; validation, writing – review & editing: EU, ML. Both authors agreed on the final version of the article.

Conflicts of interest

There are no conflicts to declare.

Data availability

Supplementary information: crystallographic details, Raman spectra, experimental details. See DOI: https://doi.org/10.1039/d5ce00956a.

Crystallographic data for all reported crystal structures has been deposited at the Cambridge Crystallographic Data Centre (CCDC) under deposition numbers 2493130–2493140.[48a–k]

Data for this article, including SCXRD datasets and Raman spectra are available at Zenodo open repository at https://doi.org/10.5281/zenodo.17432981.

Acknowledgements

Financial support from the European Research Council (ERC) under the European Union's Horizon 2020 Research and Innovation Programme (Starting Grant No. 950625), the Slovenian Research and Innovation Agency (ARIS, Project No. J1-60022), and the Jožef Stefan Institute Director's Fund is gratefully acknowledged.

Notes and references

1 M. Tramšek and B. Žemva, *Acta Chim. Slov.*, 2006, **53**, 105–116.
2 D. S. Brock, G. J. Schrobilgen and B. Žemva in *Comprehensive Inorganic Chemistry II, From Elements to Applications*, ed. J. Reedijk and K. Poeppelmeier, Elsevier, Netherlands, 2013, vol. 1, pp. 755–822.
3 N. Bartlett and F. O. Sladky, *J. Am. Chem. Soc.*, 1968, **90**, 5316–5317.
4 B. Žemva, *Croat. Chem. Acta*, 1988, **61**, 163–187.
5 G. Tavčar and M. Tramšek, *J. Fluorine Chem.*, 2015, **174**, 14–21.
6 J. G. Malm, H. Selig, J. Jortner and S. A. Rice, *Chem. Rev.*, 1965, **65**, 199–236.
7 S. S. Nabiev and I. I. Ostroukhova, *Spectrochim. Acta, Part A*, 1993, **49**, 1537–1546.
8 S. S. Nabiev, *Russ. Chem. Bull.*, 1998, **47**, 535–559.

9 S. M.-J. Yeh, *PhD Thesis*, University of California, 1984, (available at: https://escholarship.org/uc/item/9b1195zf).
10 M. A. Tius, *Tetrahedron*, 1995, **51**, 6605–6634.
11 G. Schrobilgen, G. Firnau, R. Chirakal and E. S. Garnett, *J. Chem. Soc., Chem. Commun.*, 1981, 198–199.
12 N. Vasdev, B. E. Pointner, R. Chirakal and G. J. Schrobilgen, *J. Am. Chem. Soc.*, 2002, **124**, 12863–12868.
13 M. M. Nielsen and C. M. Pedersen, *Chem. Sci.*, 2022, **33**, 6181–6196.
14 M. Gerken, M. D. Moran, H. P. A. Mercier, B. E. Pointner, G. J. Schrobilgen, B. Hoge, K. O. Christe and J. A. Boatz, *J. Am. Chem. Soc.*, 2009, **131**, 13474–13489.
15 M. D. Moran, D. S. Brock, H. P. A. Mercier and G. J. Schrobilgen, *J. Am. Chem. Soc.*, 2010, **132**, 13823–13839.
16 M. Lozinšek, *PhD Thesis*, University of Ljubljana, 2013.
17 S. Aitipamula, R. Banerjee, A. K. Bansal, K. Biradha, M. L. Cheney, A. R. Choudbury, G. Desiraju, A. Dikundwar, R. Dubey, N. Duggirala, P. P. Ghogale, S. Ghosh, P. K. Goswami, N. R. Goud, R. K. R. Jetti, P. Karpinski, P. Kaushik, D. Kumar, V. Kumar, B. Moulton, A. Mukherjee, H. Mukherjee, A. S. Myerson, V. Puri, A. Ramanan, T. Rajamannar, C. M. Reddy, N. Rodriguez-Horned, R. D. Rogers, T. N. G. Row, P. Sanphui, N. Shan, A. Singh, C. C. Sun, J. A. Swift, R. Thaimattam, T. S. Thakur, R. K. Thaper, S. P. Thomas, S. Tothadi, V. R. Vangala, P. Vishweshwar, D. R. Weyna and M. J. Zaworotko, *Cryst. Growth Des.*, 2012, **12**, 2147–2152.
18 G. J. Schrobilgen and J. M. Whalen, *Inorg. Chem.*, 1994, **33**, 5207–5218.
19 B. Kalyanaraman, L. D. Kispert and J. L. Atwood, *Acta Crystallogr., Sect. B*, 1978, **34**, 1131–1136.
20 F. R. Fronczek and N. H. Fischer, CCDC 174252: Experimental Crystal Structure Determination, 2002, DOI: 10.5517/cc5vb1c.
21 C. R. Groom, I. J. Bruno, M. P. Lightfoot and S. C. Ward, *Acta Crystallogr., Sect. B: Struct. Sci., Cryst. Eng. Mater.*, 2016, **72**, 171–179.
22 M. C. Etter, J. C. MacDonald and J. Bernstein, *Acta Crystallogr., Sect. B: Struct. Sci.*, 1990, **46**, 256–262.
23 M. Lozinšek, *Acta Crystallogr., Sect. C: Struct. Chem.*, 2025, **81**, 188–192.
24 R. J. Gillespie and T. Birchall, *Can. J. Chem.*, 1963, **41**, 148–155.
25 J. Axhausen, C. Ritter, K. Lux and A. Kornath, *Z. Anorg. Allg. Chem.*, 2013, **639**, 65–72.
26 T. Saal, R. Haiges and K. O. Christe, *Dalton Trans.*, 2023, **52**, 18143–18147.
27 M. C. Bayer, N. Greither, V. Bockmair, A. Nitzer and A. J. Kornath, *Eur. J. Inorg. Chem.*, 2022, **2022**, e202200501.
28 A. Dey, P. Metrangolo, T. Pilati, G. Resnati, G. Terraneo and I. Wlassics, *J. Fluorine Chem.*, 2009, **130**, 816–823.
29 Sakshi, Y. Gupta, C. M. Robertson, P. Munshi and A. R. Choudhury, *CrystEngComm*, 2025, **27**, 478–487.
30 E. Uran and M. Lozinšek, *Acta Crystallogr., Sect. C: Struct. Chem.*, 2025, **81**, 577–583.
31 P. Gilli, L. Pretto, V. Bertolasi and G. Gilli, *Acc. Chem. Res.*, 2009, **42**, 33–44.
32 A. I. Gubin, M. Z. Buranbaev and N. N. Nurakhmetov, *Kristallografiya*, 1988, **33**, 506–508.
33 H. S. A. Elliot, J. F. Lehmann, H. P. A. Mercier, H. D. B. Jenkins and G. J. Schrobilgen, *Inorg. Chem.*, 2010, **49**, 8504–8523.
34 B. Žemva, A. Jesih, D. H. Templeton, A. Zalkin, A. K. Cheetham and N. Bartlett, *J. Am. Chem. Soc.*, 1987, **109**, 7420–7427.
35 K. Radan, E. Goreshnik and B. Žemva, *Angew. Chem., Int. Ed.*, 2014, **53**, 13715–13719 (*Angew. Chem.*, 2014, **126**, 13935–13939).
36 K. Motaln, K. Gurung, P. Brázda, A. Kokalj, K. Radan, M. Dragomir, B. Žemva, L. Palatinus and M. Lozinšek, *ACS Cent. Sci.*, 2024, **10**, 1733–1741.
37 M. R. Bortolus, H. P. A. Mercier, B. Nguyen and G. J. Schrobilgen, *Angew. Chem., Int. Ed.*, 2021, **60**, 23678–23686 (*Angew. Chem.*, 2021, **133**, 23871–23879).
38 D. S. Brock, J. J. Casalis de Puty, H. P. A. Mercier, G. J. Schrobilgen and B. Silvi, *Inorg. Chem.*, 2010, **49**, 6673–6689.
39 M. R. Bortolus, G. J. LaChapelle, H. P. A. Mercier, J. Haner and G. J. Schrobilgen, *Inorg. Chem.*, 2023, **62**, 8761–8771.
40 M. J. Hughes, D. S. Brock, H. P. A. Mercier and G. J. Schrobilgen, *J. Fluorine Chem.*, 2011, **132**, 660–668.
41 P. A. Agron, G. M. Begun, H. A. Levy, A. A. Mason, C. G. Jones and D. F. Smith, *Science*, 1963, **139**, 842–844.
42 C. J. Adams, *J. Raman Spectrosc.*, 1974, **2**, 391–397.
43 F. O. Sladky, P. A. Bulliner and N. Bartlett, *J. Chem. Soc. A*, 1969, 2179–2188.
44 K. Motaln, K. Gurung, M. Dragomir, D. Kurzydlowski, L. Palatinus and M. Lozinšek, *Inorg. Chem.*, 2025, **64**, 14968–14976.
45 K. Nakamoto, *Infrared and Raman Spectra of Inorganic and Coordination Compounds: Part A: Theory and Application in Inorganic Chemistry*, John Wiley & Sons, Hoboken, New Jersey, 2009.
46 E. K. Murthy and G. R. Rao, *J. Raman Spectrosc.*, 1988, **19**, 359–363.
47 M. Lozinšek, H. P. A. Mercier and G. J. Schrobilgen, *Angew. Chem., Int. Ed.*, 2021, **60**, 8149–8156 (*Angew. Chem.*, 2021, **133**, 8230–8237).
48 (*a*) CCDC 2493130: Experimental Crystal Structure Determination, 2025, DOI: 10.5517/ccdc.csd.cc2pp9k8; (*b*) CCDC 2493131: Experimental Crystal Structure Determination, 2025, DOI: 10.5517/ccdc.csd.cc2pp9l9; (*c*) CCDC 2493132: Experimental Crystal Structure Determination, 2025, DOI: 10.5517/ccdc.csd.cc2pp9mb; (*d*) CCDC 2493133: Experimental Crystal Structure Determination, 2025, DOI: 10.5517/ccdc.csd.cc2pp9nc; (*e*) CCDC 2493134: Experimental Crystal Structure Determination, 2025, DOI: 10.5517/ccdc.csd.cc2pp9pd; (*f*) CCDC 2493135: Experimental Crystal Structure Determination, 2025, DOI: 10.5517/ccdc.csd.cc2pp9qf; (*g*) CCDC 2493136: Experimental Crystal Structure Determination, 2025, DOI: 10.5517/ccdc.csd.cc2pp9rg; (*h*) CCDC 2493137: Experimental Crystal Structure Determination, 2025, DOI: 10.5517/ccdc.csd.cc2pp9sh; (*i*)

CCDC 2493138: Experimental Crystal Structure Determination, 2025, DOI: 10.5517/ccdc.csd.cc2pp9tj; (j) CCDC 2493139: Experimental Crystal Structure Determination, 2025, DOI: 10.5517/ccdc.csd.cc2pp9vk; (k) CCDC 2493140: Experimental Crystal Structure Determination, 2025, DOI: 10.5517/ccdc.csd.cc2pp9wl.